electronic reprint

Journal of
Applied Crystallography
ISSN 0021-8898
Editor: **Gernot Kostorz**

Small-angle X-ray scattering measurements of helium-bubble formation in borosilicate glass

Alexander Y. Terekhov, Brent J. Heuser, Maria A. Okuniewski, Robert S. Averback, Söenke Seifert and Pete R. Jemian

Journal of
Applied Crystallography
ISSN 0021-8898

Received 14 February 2006
Accepted 3 July 2006

Small-angle X-ray scattering measurements of helium-bubble formation in borosilicate glass

Alexander Y. Terekhov,[a] Brent J. Heuser,[b]* Maria A. Okuniewski,[b] Robert S. Averback,[a] Söenke Seifert[c] and Pete R. Jemian[d]

[a]Department of Materials Science and Engineering, University of Illinois, Urbana, IL 61801, USA, [b]Department of Nuclear, Plasma, and Radiological Engineering, University of Illinois, Urbana, IL 61801, USA, [c]Argonne National Laboratory, Chemistry and Materials Technology Division, Argonne, IL 60439, USA, and [d]Frederick Seitz Materials Research Laboratory, University of Illinois, Urbana, IL 61801, USA. Correspondence e-mail: bheuser@uiuc.edu

Small-angle X-ray scattering (SAXS) measurements have been performed to study helium-bubble formation in borosilicate glass. Helium was introduced by He^+ implantation over an energy range of 1 to 2 MeV to give a uniform distribution over ~1 μm depth. The implanted dose was varied from 9×10^{13} to 2.8×10^{16} ions cm^{-2}, corresponding to a local concentration range of 40 to 11200 atomic parts per million (a.p.p.m.) averaged over the implantation depth. The SAXS response was fit with the Percus–Yevick hard-sphere interaction potential to account for interparticle interference. The fits yield helium-bubble radii and helium-bubble volume fractions that vary from 5 to 15 Å and from 10^{-3} to 10^{-1}, respectively, as the dose increased from 9×10^{13} to 2.8×10^{16} cm^{-2}. The SAXS data are also consistent with maximum helium solubility with respect to bubble formation between 40 and 200 a.p.p.m. in the borosilicate glass matrix.

1. Introduction

The immobilization of radioactive actinides requires storage media capable of withstanding the radiation damage and helium introduction associated with α decay, the latter leading to bubble formation when the solubility limit is surpassed. Helium bubbles are expected to be stable with respect to the radiation damage associated with heavy-ion recoil (Okuniewski *et al.*, 2004). The formation of helium bubbles and concomitant tensile stress can lead to fracturing of a brittle matrix. This effect may be especially significant for small bubbles where the internal gas pressure is high. The solubility of helium is generally very low in solids and is of the order of 0.3 atomic parts per million (a.p.p.m.) in borosilicate glass at 1.7×10^5 Pa (He) and 693 K (Sato *et al.*, 1990) and of the order of 1 a.p.p.m. in sodium silicate glass at 1×10^5 Pa (He) over a temperature range of 300 to 500 K (Mesko *et al.*, 2000). While helium bubbles have been observed in neutron-irradiated (Sato *et al.*, 1988) and in helium-implanted (Dé *et al.*, 1976) borosilicate glass, systematic studies of helium-bubble formation have not been performed. Sato *et al.* (1988), for example, measured density changes associated with the B(n,α)Li reaction in simulated waste glass. Both swelling and shrinking were observed depending on the matrix, with the former effect saturating at $\sim 10^{26}$ reactions m^{-3}. Transmission electron microscopy (TEM) analysis of selected samples at the saturation reaction level was also performed and pores of 0.2 μm diameter (presumed by Sato *et al.* to be helium filled) were observed, independent of the sign of the density change (Sato *et al.*, 1988). Dé *et al.* (1976) also observed bubbles in borosilicate glass containing fission-product oxides simultaneously implanted with helium (at 50 keV to a dose of 10^{14} cm^{-2}) and Pb (at 200 keV to a dose of 10^{14} cm^{-2}). The simultaneous implantation was performed to mimic α decay of heavy radionuclides. Large (~10 μm) bubbles were observed with scanning electron microscopy under these conditions, but only after a 873 K anneal. Large bubbles were also observed at a helium dose of 10^{16} cm^{-2} without annealing.

Although the solubility of helium in borosilicate glass is generally known and bubbles have been observed, a systematic study of helium-bubble formation *versus* concentration has not been reported. Small-angle scattering techniques such as small-angle neutron scattering (SANS) and small-angle X-ray scattering (SAXS) are very sensitive to dilute concentrations of structural heterogeneities such as bubbles and voids. In particular, SAXS is sensitive to helium-bubble formation, even if the solubility is only surpassed locally over a thin (~1 μm) implantation layer, as in the present case. The caveat to this statement is that a high-intensity synchrotron source is required. Although SANS has been used for the study of inert gas bubbles in metals (Carsughi, 1997; Pedersen *et al.*, 1996), we know of no study of helium bubbles (in glass or any other matrix) using SAXS.

2. Experimental

The zinc titania borosilicate glass samples, of thickness ~120 μm, were supplied by Corning (product No. 0211) with the following nominal composition by weight: 0.64 SiO_2, 0.09 B_2O_3, 0.07 ZnO, 0.07 K_2O, 0.07 Na_2O, 0.03 TiO_2, 0.03 Al_2O_3. This composition corresponds to an atomic number density of 7.7×10^{22} cm^{-3}. An extended X-ray absorption scan of the sample material revealed no structure except the 9.659 keV absorption edge of Zn (the absorption edges of the other elements are below the minimum energy available at the Advanced Photon Source 12-ID beamline spectrum). Helium was implanted at high energy (1 to 2 MeV, see below) to doses ranging from 9.4×10^{13} to 1.0×10^{17} ions cm^{-2} at beam currents of 200 to 400 nA. The implantations were performed with a van de Graaf accelerator at the Frederick Seitz Materials Research Laboratory (FS-MRL). The incident helium beam was rastered across an aperture of 4.5 mm diameter to create a uniform dose profile on the sample of similar dimension. The doses were measured in real time by recording the current in a thin wire continuously swept across the beam downstream of the beam-defining aperture. The incident-beam current was calibrated against a Faraday cup measurement prior to each implantation run. Each sample either had three or eight separate implantation runs to identical dose with the incident energy varied to create a uniform, ~1 μm thick, helium concentration depth profile located ~4.5 μm below the incident surface (both sides were treated with four runs each in the case of the samples subjected to eight implantation runs). This procedure had the effect of increasing the foreground (the SAXS response from the bubbles) without increasing the background (the response from the untreated glass matrix) or reducing the sample transmission. The SAXS data presented below were normalized to the number of implantation runs. The samples were affixed to a large metal heat sink with silver paint to ensure adequate heat removal and to prevent charge buildup during implantation. The temperature increase associated with helium implantation was estimated to be less than 373 K.

The SAXS measurements presented here were performed at the Advanced Photon Source (APS) at Argonne National Laboratory using the BESSRC 12-ID and UNICAT 33-ID beamlines. The first beamline is equipped with a 15 cm by 15 cm two-dimensional position-sensitive CCD mosaic detector, beam-defining apertures, and an automatic sample changer (Seifert *et al.*, 2000). The instrument was configured for high-Q measurement (~1 m secondary flight path length) over a wavevector transfer range of $0.02 \leq Q \leq 0.7$ Å^{-1}, where $Q = (4\pi/\lambda)\sin(\theta/2)$, with wavelength λ and scattering angle θ. The incident X-ray energy was set at 9.6000 keV (λ = 1.2915 Å), just below the Zn absorption edge mentioned above. The incident-beam size was 1 mm (horizontal) by 0.2 mm (vertical). Data were collected in 2 s snapshots, with four or five snapshots per sample. The incident beam was translated slightly (~0.5 mm vertically) for each snapshot to sample the SAXS response over a larger effective area. The high-Q data were normalized to the integrated incident-beam fluence and to the sample transmission, but not placed on an absolute intensity scale.

The SAXS response at low Q, corresponding to larger scattering objects as discussed below, was measured with the ultra-small angle X-ray scattering (USAXS) instrument on the UNICAT 33-ID beamline at the APS. This beamline is equipped with a Bonse–Hart type instrument optimized for very low Q measurements (Long *et al.*, 1991). This instrument uses two channel-cut Si single crystals before and after the sample to produce and analyze, respectively, an X-ray beam with a very narrow angular divergence. The small angular divergence allows the resolution of scattered intensity at correspondingly small angles or Q values. The incident energy for the low-Q measurements was 9.5923 keV (λ = 1.2925 Å) and the beam size was 0.6 mm (vertical) by 1.0 mm (horizontal). The low-Q data were normalized to the integrated incident-beam fluence and to the sample transmission, but not placed on an absolute scale or desmeared.

3. Results

The net SAXS responses from a series of helium-implanted borosilicate glass samples with doses of 9.4×10^{13}, 4.5×10^{14}, 9.4×10^{14}, 1.5×10^{15}, 2.3×10^{15}, 9.4×10^{15}, 1.4×10^{16}, 2.0×10^{16} and 2.8×10^{16} cm^{-2} are shown in Fig. 1. The net response was determined by subtracting the SAXS response from a zero-dose sample. The inset of Fig. 1 shows an example of the foreground and background measurements for an intermediate-dose sample. These data are radial averages over the 2π azimuthal angles measured by the area detector and have been corrected for sample transmission (~40% for all samples). The recorded intensity increases systematically with

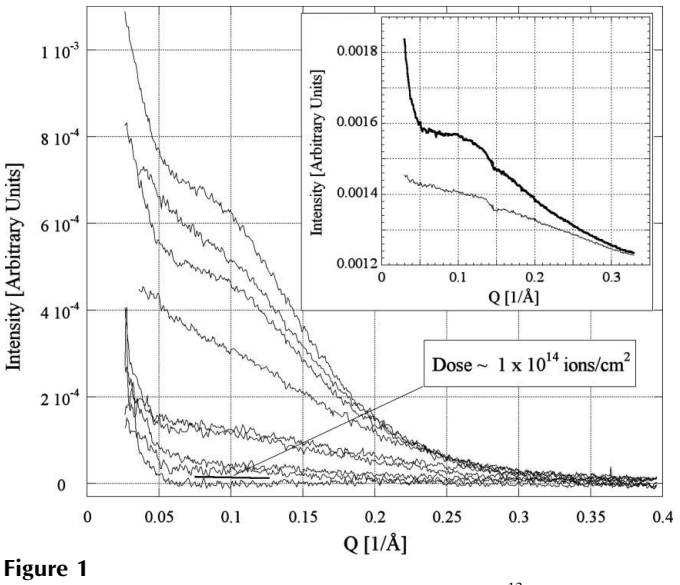

Figure 1
Net intensity *versus* Q measured at high Q for 9.4×10^{13} (bottom curve), 4.5×10^{14}, 9.4×10^{14}, 1.5×10^{15}, 2.3×10^{15}, 9.4×10^{15}, 1.4×10^{16}, 2.0×10^{16} and 2.8×10^{16} cm^{-2} (top curve) samples. The curves increase systematically with dose from bottom to top. The dose corresponding to the onset of measurable intensity at high Q is identified. The inset shows the foreground (2.3×10^{15} cm^{-2}) and background (zero-dose sample) scattering responses.

dose, as expected if the SAXS signal is from structural heterogeneities caused by helium implantation. We attribute the excess scattering to the formation of helium bubbles in the glass matrix as the solubility is surpassed. This statement is based on the success of a fitting procedure described below using a spherical form factor and a structure factor that includes interparticle interference. We note that the 4.5 μm implantation depth prevents helium loss at room temperature *via* solid-state diffusion to the free surface. Attempts to investigate the effect helium loss to the free surface by low-energy (keV) implantation were not successful.

The data in Fig. 1 indicate that the onset of significant SAXS response occurs between doses of 9.4×10^{13} and 4.5×10^{14} cm^{-2}, corresponding to a local helium concentration range of 40 to 200 a.p.p.m. The helium solubility limit with respect to detectable bubble formation in borosilicate glass is therefore between 40 and 200 a.p.p.m. The local helium concentration was calculated from the measured dose by averaging over twice the range-straggle width of the implanted-helium depth profile (∼3000 Å) obtained from a TRIM simulation (Ziegler *et al.*, 1985).

The SAXS response from the bubbles can be modeled with the single-particle form factor for a sphere averaged over a distribution of sphere radii. This model also must include interparticle interference *via* the structure factor. The Percus–Yevick hard-sphere interaction potential (Kinning & Thomas, 1984) combined with the Schulz particle size distribution function (Griffith *et al.*, 1987) was used for the fitting model. The Percus–Yevick expression represents the two-body correlation function of a hard-sphere fluid. The Schulz distribution is characterized by a mean particle size and distribution width. This distribution is asymmetric about the mean, biased toward larger particle sizes, and has been used in past analytical models for the structure factor of interacting colloids (Kotlarchyk & Chen, 1983). Fits to the SAXS data for selected doses are shown in Fig. 2. The fitting parameters include the mean sphere radius of the distribution, the distribution width, and the volume fraction of the spherical heterogeneity (the helium bubbles in this case). The dependence of the mean radius and volume fraction on implantation dose are shown in Fig. 3. Two sets of data are shown, one from the series of samples with eight implantation runs and a second series with three implantation runs. Both sample sets track together, demonstrating reasonable reproducibility. The clearest trend in these data is the systematic increase in volume fraction with dose. A less obvious trend is the increase in bubble radius with dose, at least for doses above approximately 2×10^{15} cm^{-2}.

The mean bubble radii determined from the fits to the high-Q net data are of the order of 10 Å; a logical question is if larger bubbles exist, as suggested by the previous work of Sato *et al.* (1988) and Dé *et al.* (1976). This possibility was investigated by measuring the USAXS response from samples with doses of 1.5×10^{15}, 1.4×10^{16}, 2.8×10^{16}, and 1×10^{17} cm^{-2} at low Q using the USAXS instrument on the 33-ID beamline at the APS. Note that the 1×10^{17} cm^{-2} dose sample was not measured at high Q with SAXS. The net SAXS responses for the samples implanted with doses of 1.5×10^{15}, 2.8×10^{16} and 1×10^{17} cm^{-2} are shown in Fig. 4. The low-Q measurements from the 2.8×10^{16} cm^{-2} dose and the background zero-dose samples are shown in the inset of Fig. 4. Clearly, the separation of the foreground from the zero-dose background measurement is not as great as it was at high Q. Nevertheless, excess scattering is observed for the three measurements. The net scattering response of the 1.5×10^{15} cm^{-2} sample is poorly resolved above $Q \simeq 2 \times 10^{-4}$ Å^{-1}. The net response from the 2.8×10^{16} cm^{-2} dose sample has improved counting statistics above 2×10^{-4} Å^{-1} and is slightly greater in overall magnitude. The 1×10^{17} cm^{-2} dose measurement exhibits significantly greater net intensity above $Q \simeq 2 \times 10^{-4}$ Å^{-1}. We attribute the excess scattering to the formation of larger

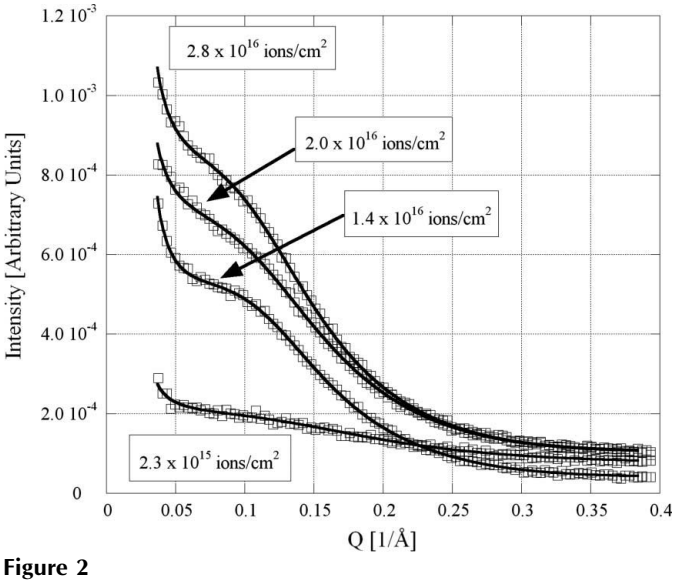

Figure 2
Fits (solid lines) to selected net high-Q measurements (open boxes) using the model scattering function described in the text.

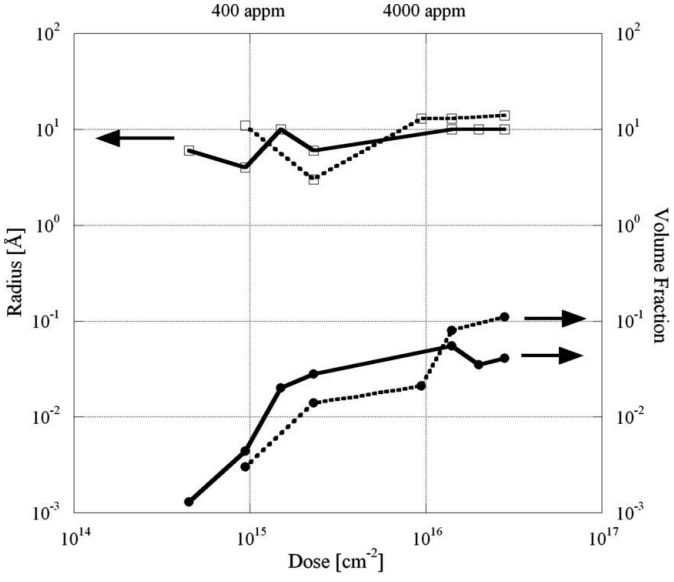

Figure 3
Helium-bubble radius and volume fraction determined from the fits of the net SAXS response. Two different data sets are shown corresponding to the three-run (solid lines) and eight-run (dotted lines) implantations.

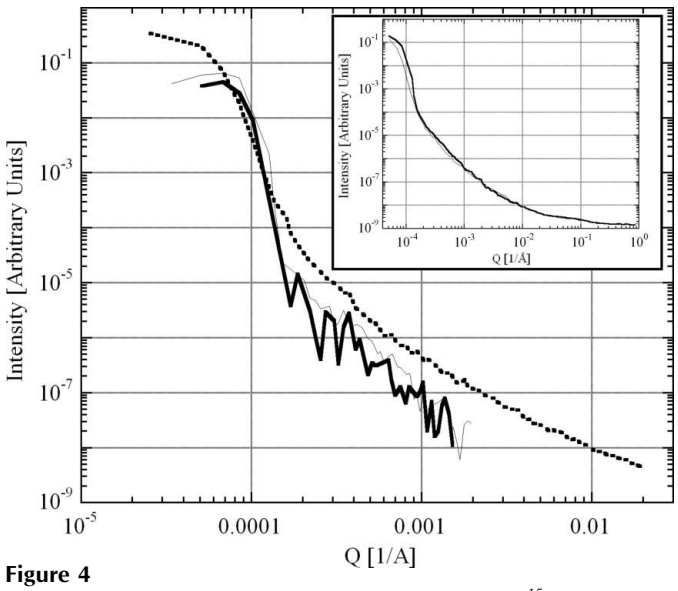

Figure 4
Net intensity *versus* Q measured at low Q for 1.5×10^{15} (dotted line), 2.8×10^{16} (thin solid line) and 1×10^{17} cm^{-2} samples (thick solid line). The truncation of the 1.5×10^{15} and 2.8×10^{16} cm^{-2} data sets above 0.002 Å^{-1} is due to very poor counting statistics. The inset shows intensity *versus* Q measured at low Q for 2.8×10^{16} cm^{-2} (thick line) and zero-dose (thin line) samples.

objects, such that Guinier response becomes resolved at lowest Q. This is discussed in the next section.

4. Discussion and summary

The high-Q SAXS response is consistent with a microstructure of small helium bubbles that grows both in radius and volume fraction with implanted dose. The onset of measurable scattering, which is assumed to coincide with initial bubble formation, occurs between doses of 9.4×10^{13} and 4.5×10^{14} cm^{-2}. If we conservatively assign the solubility limit of helium with respect to detectable helium-bubble formation at the lower value, the corresponding helium concentration is 40 a.p.p.m. This concentration corresponds to $\sim 3 \times 10^{18}$ decay events per gram of material, assuming the storage of α emitters. Such a level would be reached between 10^3 to 10^6 years for high-level waste glass and 10^2 to 10^3 years for Pu glass (Weber *et al.*, 1997). Our solubility limit is significantly higher than the limits measured by others in silicate glasses (Sato *et al.*, 1990; Mesko *et al.*, 2000). The difference could be caused by low diffusivity inhibiting the formation of bubbles at ambient temperature. In other words, room-temperature implantation may result in an initial supersaturation of helium. It could also be due to a lack of sensitivity for samples implanted with helium over a very limited depth. The SAXS measurements presented here have a volume-fraction sensitivity of the order of 10^{-3} (Fig. 3) within the 1 µm implantation depth. Although this degree of sensitivity would be difficult, if not impossible to obtain with other techniques, it may still not be adequate to resolve initial bubble formation. It is also possible that large bubbles form in advance of the small bubbles detected at high Q, but this seems counterintuitive and is inconsistent with the low-Q data.

The SAXS response from bubbles with radii greater than ~100 Å would be below the lower Q limit of the high-Q measurement and therefore undetectable. This was the reason for performing the USAXS experiments. The highest dose sample (1.0×10^{17} cm^{-2}) exhibits excess scattering in the USAXS regime that may indicate the presence of much larger, micrometre-sized helium bubbles. Two general types of scattering occur from an object at small angles: the Guinier response and the asymptotic Porod response. The Guinier response contains size information and is observed over a Q range such that $Ql \simeq 1$ is satisfied for a particle with characteristic size l (Guinier & Fournet, 1955). The Porod response is observed asymptotically at higher Q such that $Ql \gg 1$. The 1×10^{17} cm^{-2} data in Fig. 4 are indicative of a Guinier response below $Q \simeq 10^{-4}$ Å^{-1} from scattering objects of the order of 2 µm, followed by the Porod response between 10^{-4} Å^{-1} and 10^{-3} Å^{-1}. The 2 µm size estimate is derived from the $Ql \simeq 1$ condition using $Q = 5 \times 10^{-5}$ Å^{-1}, the resolution limit of the USAXS instrument used here. In fact, the shape of the curve for the 1×10^{17} cm^{-2} dose compared with the others in Fig. 4 is consistent with the growth of bubbles beyond the resolution limit as the dose approaches 1×10^{17} cm^{-2}. While such an observation would be consistent with the work of Dé *et al.* (1976), our data are inconclusive with regard to bubbles of this size since the Guinier region is at the resolution limit of the instrument.

This work was supported by the US Department of Energy, Nuclear Engineering Education Research (NEER) program under Grant No. DFG07-01-ID14121. The APS BESSRC is supported by the US Department of Energy under Contract No. W-31-109-ENG-38. The UNICAT facility at the APS is supported by the US DOE under Award No. DEFG02-91ER45439, through the UIUC FS-MRL, the Oak Ridge National Laboratory (US DOE Contract No. DE-AC05-00OR22725 with UT-Battelle LLC), the National Institute of Standards and Technology (US Department of Commerce) and UOP LLC. The APS is supported by the US DOE, Basic Energy Sciences, Office of Science under Contract No. W-31-109-ENG-38. This material is based upon work supported by the US Department of Energy, Division of Materials Sciences, under Award No. DEFG02-91ER45439, through the FS-MRL at the University of Illinois at Urbana–Champaign. The use of the BESSRC, UNICAT and FS-MRL facilities is gratefully acknowledged.

References

Carsughi, F. (1997). *Bull. Mater. Sci.* **20**, 467–474.
Dé, A. K., Luckscheiter, B., Lutze, W., Malow, G. & Schiewer, E. (1976). *Am. Ceram. Soc. Bull.* **55**, 500–503.
Griffith, W. L., Triolo, R. & Compere, A. L. (1987). *Phys. Rev. A*, **35**, 2200–2206.
Guinier, A. & Fournet, G. (1955). *Small-Angle Scattering of X-rays*. New York: John Wiley.
Kinning, D. J. & Thomas, E. L. (1984). *Marcomolecules*, **17**, 1712–1718.
Kotlarchyk, M. & Chen, S.-H. (1983). *J. Chem. Phys.* **79**, 2461–2469.

Long, G. G., Jemian, P. R., Weertman, J. R., Black, D. R., Burdette, H. E. & Spal, R. (1991). *J. Appl. Cryst.* **24**, 30–37.
Mesko, M. G., Newton, K. & Shelby, J. E. (2000). *Phys. Chem. Glasses*, **31**, 111–116.
Okuniewski, M. A., Ashkenazy, Y., Heuser, B. J. & Averback, R. S. (2004). *J. Appl. Phys.* **96**, 4181–4188.
Pedersen, J. S., Horsewell, A. & Eldrup, M. (1996). *J. Phys. Condens. Matter*, **8**, 8431–8455.
Sato, S., Furuya, H., Kozaka, T., Inagaki, Y. & Tamai, T. (1988). *J. Nucl. Mater.* **152**, 265–269.
Sato, S., Furuya, H., Morikawa, K., Sugisaki, M. & Inagaki, Y. (1990). *J. Nucl. Sci. Technol.* **27**, 343–349.
Seifert, S., Winans, R. E., Tiede, D. M. & Thiyagarajan, P. (2000). *J. Appl. Cryst.* **33**, 782–784.
Weber, W. J., Ewing, R. C., Angell, C. A., Arnold, G. W., Cormack, A. N., Delaye, J. M., Griscom, D. L., Hobbs, L. W., Navrotsky, A., Price, D. L., Stoneham, A. M. & Weinberg, M. C. (1997). *J. Mater. Res.* **12**, 1946–1978.
Ziegler, J. F., Biersack, J. P. & Littmark, U. (1985). *The Stopping Power and Range of Ions in Solids*. New York: Pergamon Press.